How Water Meets a Hydrophobic Surface

Adelé Poynor, Liang Hong, Ian K. Robinson, and Steve Granick
Materials Research Laboratory, University of Illinois, Urbana, Illinois 61801, USA

Zhan Zhang and Paul A. Fenter
Chemistry Division, Argonne National Laboratory, Argonne, Illinois 60439, USA
(Received 12 July 2006; published 27 December 2006)

Synchrotron x-ray reflectivity measurements of the interface between water and methyl-terminated octadecylsilane monolayers with stable contact angle $>100°$ conclusively show a depletion layer, whether or not the water is degassed. The thickness is of order one water molecule: 2–4 Å with electron density $<40\%$ that of bulk water. Considerations of coherent and incoherent averaging of lateral inhomogeneities show that the data cannot be explained by ''nanobubbles.'' When the contact angle is lower, unstable in time, or when monolayers fail to be sufficiently smooth over the footprint of the x-ray beam, there is no recognizable depletion.

DOI: 10.1103/PhysRevLett.97.266101 PACS numbers: 68.08.−p, 82.70.Uv

The literature is conflicting whether water, meeting an extended hydrophobic solid, forms a thermodynamically driven low-density depletion layer [1–6]. This problem of hydrophobicity at extended surfaces has significant implications for protein folding [4,5,7], for the boundary condition when fluids flow past hydrophobic surfaces in microchannels [8–10], and even for geosciences because many clays in soils are hydrophobic. Previous experiments have been interpreted sometimes in favor of a depletion layer [11–16], sometimes against [17–19], and sometimes as indicating intimate solid-water contact in places and ''nanobubbles'' in others [20,21]. This experimental Letter concerns understanding this and will not address the theoretical controversies.

The experimental ambiguities stem partially from different interpretations of what it means to have a hydrophobic surface. We therefore address the most favorable situation, methyl-terminated organic monolayers of the best quality that we can synthesize: contact angle $>100°$ against water, rms roughness <0.2 nm, and a thickness which remains the same in air and ethanol, as measured with ellipsometry, demonstrating chemical robustness of the monolayer. Monolayers of this key high contact angle were studied as Seo and Satija have shown [19] the absence of depletion when water meets polystyrene, a more polar substance whose advancing contact angle against water is $\approx 90°$. Surfactant-coated surfaces were used in some earlier studies, but selection of a chemically attached monolayer circumvents the potential complication that surfactant-coated solid surfaces may reconstruct to form new morphologies when placed in water [22]. Silane monolayers can be prone to defects, however [23], and this also was our experience (see below). Another distinctive aspect of this study is that we used water deaerated to the best of our ability, minimizing the chance that gas would segregate to the surface from the bulk water. Third, we avoid using a potentially perturbative mechanical probe microscopy such as atomic force microscope (AFM).

For characterization, we use specular synchrotron x-ray reflectivity, as it has subnanometer thickness resolution. This study probed a range of momentum transfers up to 0.8 $Å^{-1}$, providing a threefold to fivefold better vertical (out-of-plane) spatial resolution than previous neutron-based studies.

Self-assembled methyl-terminated octadecyl chains of condensed octadecyltriethoxysiloxane (OTE) were deposited on oxidized $\langle 100 \rangle$ silicon wafers using methods described previously [24]. The water was first passed through a Barnstead Nanopure II deionizing system. For deaeration, it was subjected to 5–7 pump-freeze-thaw cycles. In control experiments deaerated water was also prepared by boiling and subsequent cooling in a sealed container, without a noticeable difference in findings. The monolayers were characterized by contact angle measurement and AFM; samples were discarded unless AFM showed a smooth monolayer essentially free of aggregates, with the roughness and contact angle criteria noted above. To achieve monolayers of this high quality required that the OTE be distilled before use. When the criteria of smoothness and high contact angle were not satisfied, experiments failed to display the distinct x-ray interferences that are directly associated with the depletion layer that we analyze below.

Specular reflectivity, R (i.e., the ratio of reflected to incident x-ray flux as a function of incident angle α) is related directly to the electron density profile $\rho(z)$ in the surface-normal direction by the ''master formula,'' $R \propto |\int \rho(z) e^{iQz} dz|^2$ [25]. The x-ray measurements were performed at the Advanced Photon Source (BESSRC/XOR beam line 12-BM) at Argonne National Laboratory. The temperature was ambient, 23–25 °C. The 25 mm long sample was held in a ''thin-film'' cell such that an 8 μm thick Kapton membrane confined a ≈ 2 μm thick water layer [26]. The sample cell was assembled underwater to ensure that no air bubbles were trapped under the Kapton film. The x-ray beam was reflected at incident angles α,

generally ranging from 0.1° to 2.3° [corresponding to momentum transfers of $Q = (4\pi/\lambda)\sin(\alpha)$ of 0.03 $Å^{-1}$ to 0.8 $Å^{-1}$] with incident beam sizes ranging from 0.04 mm to 0.4 mm so that the resulting beam footprint remained well within the surface boundary. A monochromatic x-ray beam ($E = 19.0$ keV) was used to maximize the transmission through the water layer, with a full incident beam flux of 2×10^{10} photons/ sec. Specular reflectivity measurements took place within 20 min for a given beam spot with two additional scans to probe the background with the sample angle offset by $\pm 0.05°$, during which time no changes in the reflected intensity were observed. Experiments using higher energy x rays and thicker water layers resulted in beam damage, and are not reported here. A correction was applied to the data for angle-dependent attenuation by the water and Kapton layers [26] and an overall scale factor was used in the data analysis.

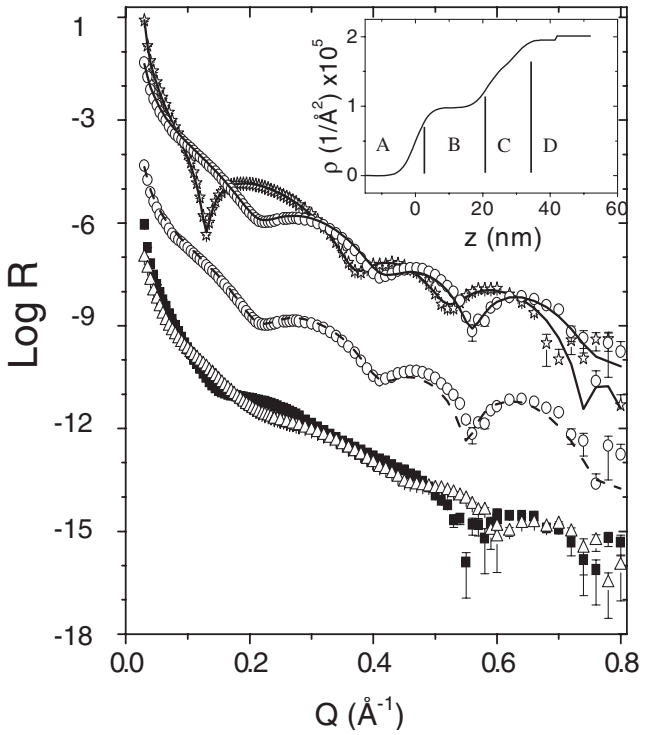

FIG. 1. X-ray reflectivity curves for an OTE monolayer on an oxidized ⟨100⟩ silicon wafer in air (open stars) and water (open circles). Solid lines through the data show the best fits. For comparison, the extreme of acceptable fit is illustrated by the dashed line and is compared to the experimental curve taken in water (these curves are shifted down 3 decades for clarity). For comparison, x-ray reflectivity curves for a low-quality OTE monolayer are also shown when this hydrophobic surface is exposed to air (solid squares) and ambient water (open triangles). These curves are shifted down six decades for clarity; it was not possible to fit data for these low-quality monolayers using the PARRAT formalism used elsewhere in this Letter. The inset shows a schematic representation of electron density as a function of location in different regions, separated schematically by vertical lines: *A* (air), *B* (OTE alkyl chains), *C* (OTE head group), *D* (silicon and silicon oxide).

To fix parameters for subsequent analysis, the monolayers were first studied in ambient air (see Fig. 1). The reflectivity shows sharp dips and oscillations owing to interference between x rays reflected at the silicon-organic and organic-air interfaces, and is thus highly sensitive to the monolayer thickness D. The first intensity dip gives a rough estimate of the thickness D: $D = \pi/Q_{\min} \approx$ 24–25 Å, where the range depends on the sample. This is in excellent agreement with the landmark study by Tidswell *et al.* of octadecylsilane monolayers in air [27]. Figure 1 shows the derived electron density profile corresponding to the best-fit reflectivity. It includes contributions not only from the monolayer thickness and density but also from interfacial oxide and monolayer head group layers. The observation of deep intensity minima shows decidedly that the monolayers were homogeneous over the large area probed by the x-ray beam.

When the hydrophobic monolayer was immersed in water, intensity dips persisted but at different location and magnitude. This monolayer-water interface would be almost invisible (i.e., no intensity dips for $Q < 0.3$ $Å^{-1}$) if there were no density depletion at the monolayer-water interface, as the electron density of water and the organic film are nearly the same. The dip positions of the reflectivity interference oscillations shifted to a much larger momentum transfer ($Q_{\min} \sim 0.2$ $Å^{-1}$) than in air. It makes no sense physically to suppose a reduced monolayer thickness, $D = \pi/Q_{\min} \approx 14$ Å, i.e., $<2/3$ the thickness of these same monolayers in air. The reason is more interesting: because electron density profile normal to the monolayer-water interface varied nonmonotonically, the phase of the interference shifted because electron density passed through a region whose electron density was less than either bulk water or monolayer. The derived electron density for the monolayer-water interface is shown in Fig. 2.

For quantification, least-squares comparisons between experimental and calculated reflectivities were made using the widely used PARRAT formalism [28], in which interfacial electron density is modeled with a series of error function profiles [26,27]. Fits of monolayers in air fixed parameters used to fit reflectivity of these same monolayers immersed in water, including the thicknesses, scattering length densities, and roughnesses for silicon oxide and bulk silicon layers. An important parameter determining quality of fit was the standard deviation of the electron density profile of the organic monolayer surface, 7.1 Å (fixed from measurements in air); note that this measure of interfacial smoothness exceeds the 2 Å width measured by AFM. When (below) we quote thickness of the depletion layer between bulk water and hydrophobic monolayer, we refer to distance between the middle of the error functions that defined the locations of these surfaces.

Figure 2 compares findings from experiments where the water was saturated with atmospheric gas, or deaerated. The comparison involves independent experiments using

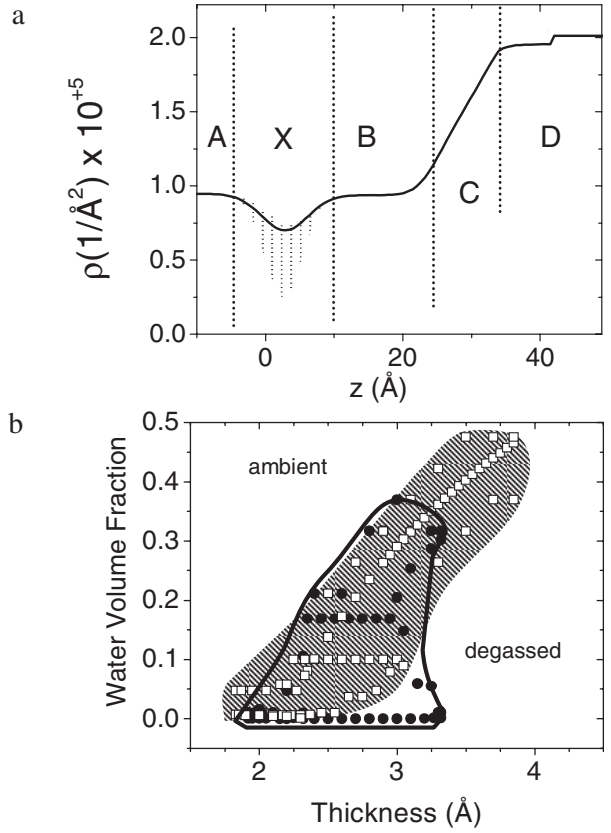

FIG. 2. (a) Schematic representation of the scheme to derive the electron density profile of the hydrophobic monolayer immersed in water. Labels distinguish the different regions, separated schematically by vertical lines: *A* is the bulk water, *X* is the hypothetical depletion layer, *B* is the OTE, *C* is the OTE head group and roughness, and *D* is the silicon substrate. For clarity, schematic representation of width of electron density deficit in region *X* is exaggerated beyond the actual values summarized in (b). (b) The depletion layer thickness and water volume fraction, obtained using the PARRAT formalism [28], were found to be consistent with a range of possible models. The hatched area and black curve represent the range of acceptable parameter values to describe the low-density region for two samples immersed in degassed water and ambient water, respectively, determined by sampling the quality of fit at points indicated by the black circles and white squares.

different organic monolayers. Within a range of fits almost equally consistent with both sets of data, we infer a 2–4 Å thick depletion region with density 0–40% of the equivalent water density. Acceptable fits for different combinations of parameters arise because thickness and electron density relative to the bulk are strongly coupled in modeling. We note that the experiment was most sensitive to the product of the magnitude and width of density depletion which was nearly constant indicating that a depletion region is necessary to explain these data. The derived density profile does not show a zero-density region, even when including a 2 Å thick density gap, because the plotted profile includes the effect of surface roughness which smears out this laterally averaged interfacial density profile along the surface-normal direction. In Fig. 2(b), we note with interest that from independent experiments employing different samples, a consistent depletion layer thickness was found whether the water was saturated with ambient gases or deaerated.

Parenthetically, the depletion thickness reported in Fig. 2(b) must be regarded as an upper bound, although the existence of the depletion layer is unequivocal. This is because protons on the methyl-terminated hydrophobic monolayer and on water adjoining the monolayer are virtually invisible. We do not seek to account for this at the present time as quantification of the radii of the methyl protons appears to be subjective.

Given the inconsistencies among prior studies, it is reasonable to ask whether or not this depletion layer cushions the hydrophobic surface uniformly or whether ''bubbles'' are admitted. These x-ray data afford a succinct quantitative test of this, as summarized in Fig. 3. There are two possibilities to consider, depending on whether the hypothetical lateral size of putative bubbles is larger than or less than the momentum transfer resolution of the x-ray measurement, ~500 Å high in the vertical direction and 850 Å in the transverse direction. Previous observations indicated bubbles 200–300 Å high and ~2000 Å in lateral dimension [20]. The present measurements would allow objects ~500 Å high to be observed, e.g., as additional oscillations in the reflectivity profiles, but no evidence for such objects was seen. We also consider the impact of such objects on the reflectivity profiles in the case where they are vertically larger. Here, the sensitivity to such objects depends upon our lateral resolution. If these lateral variations in structure are coherently averaged this would reduce the effective water density near the interface. This will result in an intensity dip position unchanged with respect to the monolayer in air with only reduced magnitude of the density oscillation. If the lateral size of the bubble is substantially larger and necessitates incoherent averaging of the two reflectivity profiles, the deep intensity minimum observed for the monolayer in air will be preserved, but this too is inconsistent with data in Fig. 3. Together these observations allow us to rule out ''nanobubbles'' as playing a significant role in these observations.

In summary, the synchrotron x-ray data reported here unambiguously confirm the theoretical expectation that water, when it meets a planar hydrophobic surface, forms a depletion layer [1,2]. We obtain a substantially narrower limit on the range of acceptable thicknesses than previously achieved and show that deaerated water, and water saturated with ambient gases result in consistent interfacial structures. When the necessary conditions of sample quality were not met, no effect was observed. An earlier study that found a much larger influence of dissolved gas [13] was based on data with a substantially poorer vertical resolution (due to a narrower Q range) than was achieved in this study.

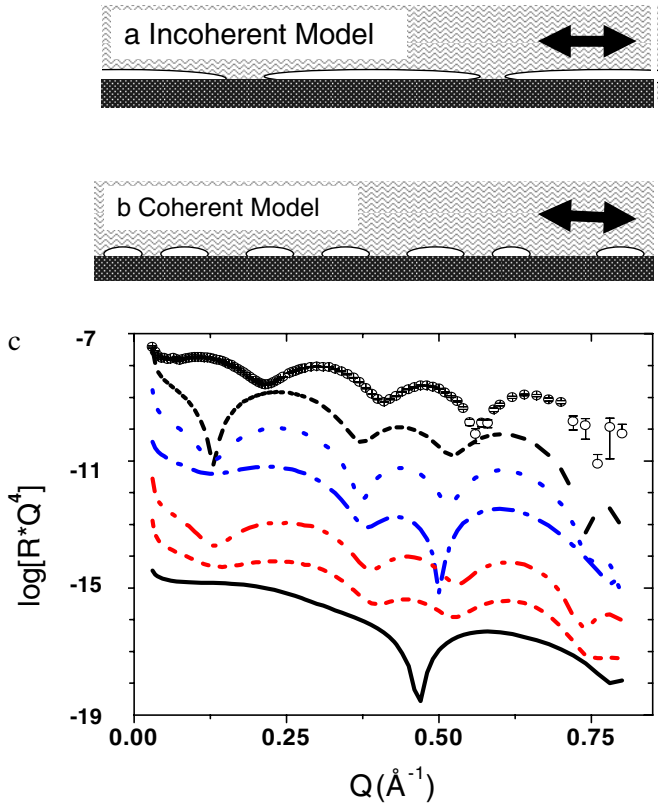

FIG. 3 (color online). Schematic diagram of the nanobubble model in which the x-ray reflectivity in water for self-assembled organic monolayers (Fig. 2) is obtained by (a) incoherently, and (b) coherently averaging the reflectivity from a planar hydrophobic monolayer in contact with bulk water vs air. Incoherent scattering occurs when the characteristic size of the bubbles is larger than the x-ray coherence length of approximately 850 Å, indicated by the two-sided arrow, while coherent scattering occurs when the characteristic size of the bubbles is less than the x-ray coherence length. (c) Normalized reflectivity RQ^4 is plotted against Q on semilogarithmic scales. The open symbols are data. The dashed black line is the calculated fit for 0% surface coverage of water. The dotted and dash-dotted lines (blue online) are coherently calculated curves for 30% and 70% water surface coverage, respectively. The dot-dash-dotted and the short-dashed lines (red online) are incoherently calculated curves for 30% and 70% water surface coverage, respectively. The solid line is a calculation for 100% water surface coverage. The calculations are offset vertically for clarity.

We thank Yan Yu and Wina Tjen for assistance in monolayer preparation, and the Hahn-Meitner-Institut Berlin GmbH for use of PARRATT32 software. Partial support was provided through the Science and Technology Center for Purification of Water, NSF No. CTS-0120978. This work was supported by the U.S. Department of Energy (both through the Geosciences Research Program and through its support of the APS) through Contract No. W-31-109-ENG-38 to Argonne National Laboratory, and by No. DEFG02-02ER46019 to the University of Illinois at Urbana-Champaign.

[1] F. H. Stillinger, J. Solution Chem. **2**, 141 (1973).
[2] K. Lum, D. Chandler, and J. D. Weeks, J. Phys. Chem. B **103**, 4570 (1999).
[3] D. M. Huang and D. Chandler, J. Phys. Chem. B **106**, 2047 (2002).
[4] X. H. Huang, R. H. Zou, and B. J. Berne, J. Phys. Chem. B **109**, 3546 (2005).
[5] P. Liu, X. H. Huang, R. H. Zhou, and B. J. Berne, Nature (London) **437**, 159 (2005).
[6] H. S. Ashbaugh and L. R. Pratt, Rev. Mod. Phys. **78**, 159 (2006).
[7] D. M. Huang and D. Chandler, Proc. Natl. Acad. Sci. U.S.A. **97**, 8324 (2000).
[8] I. Vinogradova, Int. J. Miner. Process. **56**, 31 (1999).
[9] Y. Zhu and S. Granick, Phys. Rev. Lett. **88**, 106102 (2002).
[10] P.-G. de Gennes, Langmuir **18**, 3413 (2002).
[11] R. Steitz, T. Gutberlet, T. Hauss, B. Klösgen, R. Krastev, S. Schemmel, A. C. Simonsen, and G. H. Findenegg, Langmuir **19**, 2409 (2003).
[12] D. Schwendel, T. Hayashi, R. Dahint, A. Pertsin, M. Grunze, R. Steitz, and F. Schreiber, Langmuir **19**, 2284 (2003).
[13] D. A. Doshi, E. B. Watkins, J. N. Israelachvili, and J. Majewski., Proc. Natl. Acad. Sci. U.S.A. **102**, 9458 (2005).
[14] Z. B. Ge, D. G. Cahill, and P. V. Braun, Phys. Rev. Lett. **96**, 186101 (2006).
[15] L. B. R. Castro, A. T. Almeida, and D. F. S. Petri, Langmuir **20**, 7610 (2004).
[16] T. R. Jensen, M. O. Jensen, N. Reitzel, K. Balashev, G. H. Peters, K. Kjaer, and T. Bjørnholm, Phys. Rev. Lett. **90**, 086101 (2003).
[17] Y. Takata, J. H. J. Cho, B. M. Law, and M. Aratoni, Langmuir **22**, 1715 (2006).
[18] M. Mao, J. H. Zhang, R. H. Yoon, and W. A. Ducker, Langmuir **20**, 1843 (2004).
[19] Y. S. Seo and S. Satija, Langmuir **22**, 7113 (2006).
[20] J. W. G. Tyrrell and P. Attard, Phys. Rev. Lett. **87**, 176104 (2001).
[21] N. Ishida, T. Inoue, M. Miyahara, and K. Higashitani, Langmuir **16**, 6377 (2000).
[22] H. N. Patrick, G. G. Warr, S. Manne, and I. A. Aksay, Langmuir **15**, 1685 (1999).
[23] OTS (octadecyltrichlorosilane) domains, slightly thicker in water than air, have been noticed in AFM experiments, suggesting swelling [18]. Based on neutron reflectivity, defects in OTS layers on silicon were also reported; T. L. Kuhl *et al.*, Biophys. J. **75**, 2352 (1998).
[24] J. Peanasky, H. M. Schneider, S. Granick, and C. R. Kessel, Langmuir **11**, 953 (1995).
[25] J. Als-Nielsen and D. McMorrow, *Elements of Modern X-Ray Physics* (Wiley, New York, 2001).
[26] P. Fenter, Rev. Mineral. Geochem. **49**, 149 (2003).
[27] I. M. Tidswell, T. A. Rabedeau, P. S. Pershan, and S. D. Kosowsky, J. Chem. Phys. **95**, 2854 (1991).
[28] G. Parratt, Phys. Rev. **95**, 359 (1954).